Magnetic properties of a novel family of ferrous cubanes

Electronic Supplementary Information

Francesco Piga[a], **Fabrizio Moro**[a], **Itana Krivokapic**[a], **Alexander J. Blake**[a], **Ruth Edge**[b], **Eric J.L. McInnes**[b], **David J. Evans**[c], **Jonathan McMaster**[a], **Joris van Slageren**[a,d,*]

[a] *School of Chemistry, University of Nottingham, University Park, Nottingham, NG7 2RD, United Kingdom.*
[b] *School of Chemistry, The University of Manchester, Manchester, M13 9PL, United Kingdom.*
[c] *Department of Biological Chemistry, John Innes Centre, Norwich Research Park, Norwich, NR4 7UH, United Kingdom.*
[d] *Institut für Physikalische Chemie, Universität Stuttgart, Pfaffenwaldring 55, D-70569 Stuttgart, Germany. Tel: +49(0)71168564380; E-mail: slageren@ipc.uni-stuttgart.de.*

1. Experimental Details

All syntheses and manipulations were carried out by using Schlenk techniques; all solvents used in syntheses were freshly distilled under dinitrogen. Synthesis of **1**: The addition of hmpH (1.114 g, 10 mmol) in MeOH (10 ml) to anhydrous $FeCl_2$ (1.274 g, 10 mmol) in MeOH (20 ml), followed by NaOMe (0.551 g, 10 mmol) in 30 ml MeOH yielded an orange solution that was heated to reflux for 30 min and filtered while still hot. Large orange block-like X-ray quality crystals of **1** form after slow cooling of the filtrate. Anal. (%) Calcd for $C_{28}H_{40}N_4Fe_4O_8Cl_4$: C, 36.32; H, 4.35; N, 6.05. Found: C, 36.29; H, 4.47; N, 5.87. IR (Nujol, cm^{-1}): 1737m, 1726m, 1699w, 1674m, 1531s, 1406w, 1359m, 1313s, 1240m. Synthesis of **2**: The addition of hmpH (1.114 g, 10 mmol) in EtOH (10 ml) to anhydrous $FeCl_2$ (1.274 g, 10 mmol) in EtOH (20 ml), followed by NaOEt [obtained from the reation of *n*-butyllithium (10 mmol in 4 mL hexanes) with EtOH (30 ml)] yielded an orange solution that was heated to reflux for 30 min and filtered while still hot. Large orange block-like X-ray quality crystals **of 2** form after slow cooling of the filtrate. Anal. (%) Calcd for $C_{32}H_{48}N_4Fe_4O_8Cl_4$: C, 39.14; H, 4.93; N, 5.71. Found: C, 39.19; H, 5.12; N, 5.60. IR (Nujol, cm^{-1}): 1737w, 1697w, 1677m, 1531s, 1405m, 1359m, 1314s, 1240m.

Crystallographic data for **1** and **2** were collected on a Bruker SMART APEX diffractometer using graphite-monochromated Mo *K*α radiation (λ = 0.71073 Å). Both structures were solved by direct methods and refined against all data using SHELXL97.[1] Crystal data for **1**: $C_{28}H_{40}N_4Fe_4O_4Cl_4$, M = 925.84, tetragonal space group $I\bar{4}2d$, Z = 8, a = b = 16.0765(6) Å, c = 29.839(2) Å, α = β = γ = 90°, V = 7712.1(7) $Å^3$, T = 90(2) K, μ = 1.801 mm^{-1}, R_1 = 0.0387, wR_2 = 0.0993. Crystal data for **2**: $C_{32}H_{48}N_4Fe_4O_4Cl_4$, M = 981.94, orthorombic space group P*bca*, Z = 8, a = 16.8291(6) Å, b = 16.4962(6) Å, c = 29.6189(10) Å, α = β = γ = 90°, V = 8222.69 $Å^3$, T = 90(2) K, μ = 1.694 mm^{-1}, R_1 = 0.0295, wR_2 = 0.0729. CCDC 820008 (**1**), CCDC 820009 (**2**).

Magnetic data for **1** and **2** were recorded on a Quantum Design MPMS-XL5 SQUID magnetometer on powder samples in compressed Teflon pellets. Data were corrected for the diamagnetic contribution using Pascal's constants. W-Band EPR spectra were recorded on a Bruker Elexsys spectrometer. A homebuilt spectrometer based on a Jasco J815 spectrometer and an Oxford Instruments SM4000 8T spectromag optical split coil magnet was used for MCD measurements. Mössbauer spectra were recorded in the solid state, at 80 K, in zero magnetic field using a ^{57}Co source (205 MBq) in a rhodium matrix on an ES-Technology MS105 spectrometer. The sample was prepared by grinding with boron nitride before loading into the sample holder. The spectrum was fitted with Lorentzian lines and referenced against natural iron foil (25 μm) at 298 K.

2. Crystallography

Figure S1 displays the two independent molecules in the unit cell of **1**. All iron ions of each molecule are symmetry-equivalent. Table S1 reports selected bond distances and angles. Figure S2 depicts the crystal structure of **2**, which possesses one molecule in the unit cell. All iron ions are crystallographically distinct. Table S2 lists selected bond angles and distances.
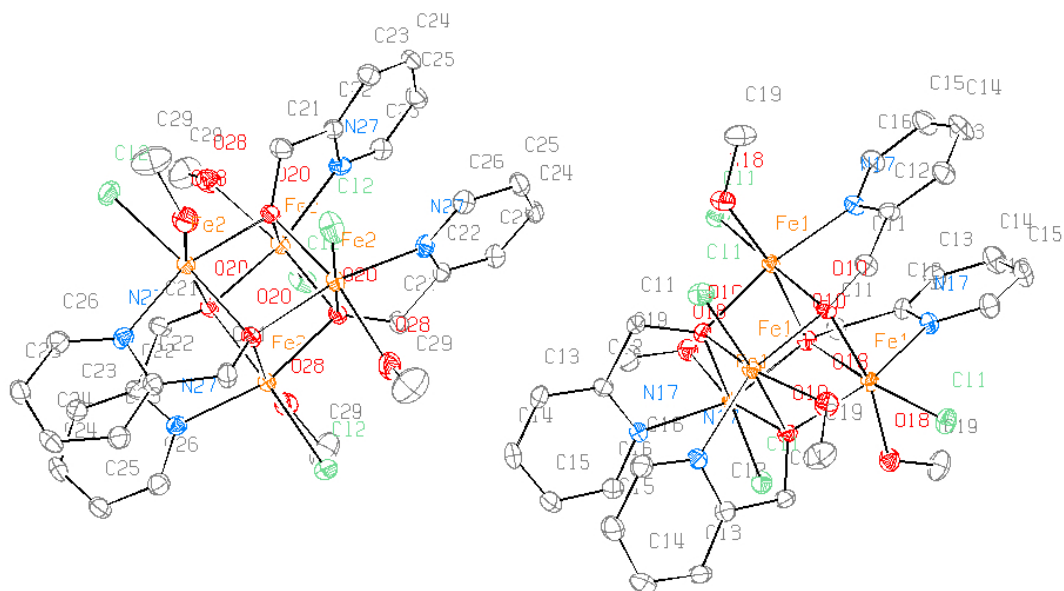
Figure S1. Crystal structure of [Fe(hmp)(MeOH)Cl]$_4$ (complex **1**).

Table S1. Selected bond distances and angles for complex **1**.

Atom 1	Atom 2	Length (Å)	Atom 1	Atom 2	Atom 3	Angle (°)
Fe1	Cl1	2.405(1)	Fe1	O10	Fe1	98.9(1)
Fe1	N17	2.155(3)	Fe1	O10	Fe1	97.6(1)
Fe1	O18	2.191(3)	Fe1	O10	Fe1	96.2(1)
Fe1	O10	2.117(3)	O10	Fe1	O10	80.85(9)
Fe1	O10	2.109(2)	O10	Fe1	O10	81.86(9)
Fe1	O10	2.163(3)	O10	Fe1	O10	83.0(1)
Fe2	Cl2	2.408(1)	Fe2	O20	Fe2	99.9(1)
Fe2	N27	2.160(3)	Fe2	O20	Fe2	95.9(1)
Fe2	O28	2.199(3)	Fe2	O20	Fe2	97.6(1)
Fe2	O20	2.121(3)	O20	Fe2	O20	79.9(1)
Fe2	O20	2.112(3)	O20	Fe2	O20	83.1(1)
Fe2	O20	2.178(3)	O20	Fe2	O20	81.7(1)

Figure S2. Crystal structure of $[Fe(hmp)(EtOH)Cl]_4$ (complex **2**).

Table S2. Selected bond distances and angles for complex **2**.

Atom 1	Atom 2	Length (Å)	Atom 1	Atom 2	Atom 3	Angle (°)
Fe1B	Cl2B	2.4112(6)	Fe1B	O18B	Fe1A	98.99(5)
Fe1B	N11B	2.164(2)	Fe1B	O18A	Fe1A	99.54(5)
Fe1B	O21B	2.187(2)	Fe1B	O18A	Fe1D	96.08(5)
Fe1B	O18B	2.112(1)	Fe1B	O18D	Fe1D	97.36(5)
Fe1B	O18D	2.115(1)	Fe1B	O18B	Fe1C	98.29(5)
Fe1B	O18A	2.162(1)	Fe1B	O18D	Fe1C	96.19(5)
Fe1C	Cl2C	2.4016(6)	Fe1A	O18A	Fe1D	98.04(5)
Fe1C	N11C	2.169(2)	Fe1A	O18C	Fe1D	96.67(5)
Fe1C	O21C	2.179(1)	Fe1A	O18B	Fe1C	96.47(5)
Fe1C	O18C	2.115(1)	Fe1A	O18C	Fe1C	98.95(5)
Fe1C	O18B	2.117(1)	Fe1C	O18D	Fe1D	98.89(5)
Fe1C	O18D	2.182(1)	Fe1C	O18C	Fe1D	99.48(5)
Fe1D	Cl2D	2.4084(6)	O18C	Fe1A	O18B	80.71(5)
Fe1D	N11D	2.169(2)	O18C	Fe1C	O18B	82.19(5)
Fe1D	O21D	2.166(2)	O18C	Fe1A	O18A	82.48(5)
Fe1D	O18D	2.120(1)	O18C	Fe1D	O18A	81.12(5)
Fe1D	O18A	2.115(1)	O18B	Fe1A	O18A	80.10(5)
Fe1D	O18C	2.170(1)	O18B	Fe1B	O18A	80.79(5)
Fe1A	Cl2A	2.3930(6)	O18D	Fe1B	O18A	82.03(5)
Fe1A	N11A	2.167(2)	O18A	Fe1D	O18D	83.02(5)
Fe1A	O21A	2.182(1)	O18D	Fe1C	O18C	80.42(5)
Fe1A	O18A	2.118(1)	O18C	Fe1D	O18D	80.59(5)
Fe1A	O18C	2.108(1)	O18D	Fe1B	O18B	82.92(5)
Fe1A	O18B	2.186(1)	O18B	Fe1C	O18D	81.20(5)

2. Mössbauer Spectroscopy

Mössbauer spectra (Figures S3 and S4) were recorded in the solid state, at 80 K, in zero magnetic field using a ^{57}Co source (205 MBq) in a rhodium matrix on an ES-Technology MS105 spectrometer. The samples were prepared by grinding with boron nitride before loading into the sample holder. The spectra were fit with Lorentzian lines and referenced against natural iron foil (25 μm) at 298 K. Both spectra can be fitted with a one doublet model, or with a two doublets model with the doublets either overlapped or nested (Table S3 and S4). In both cases, the best fit is obtained with two nested doublets, with identical isomer shifts and slightly different quadrupole splittings; this suggests the presence of two different iron sites with a slightly different environment. The values of isomer shift and quadrupole splitting are consistent with those reported for high-spin iron(II) complexes[2]. In the case of **2**, the signal from a small impurity has also been fitted, and attributed to high-spin iron(III)[2], probably deriving from an accidental exposure of the sample to air.
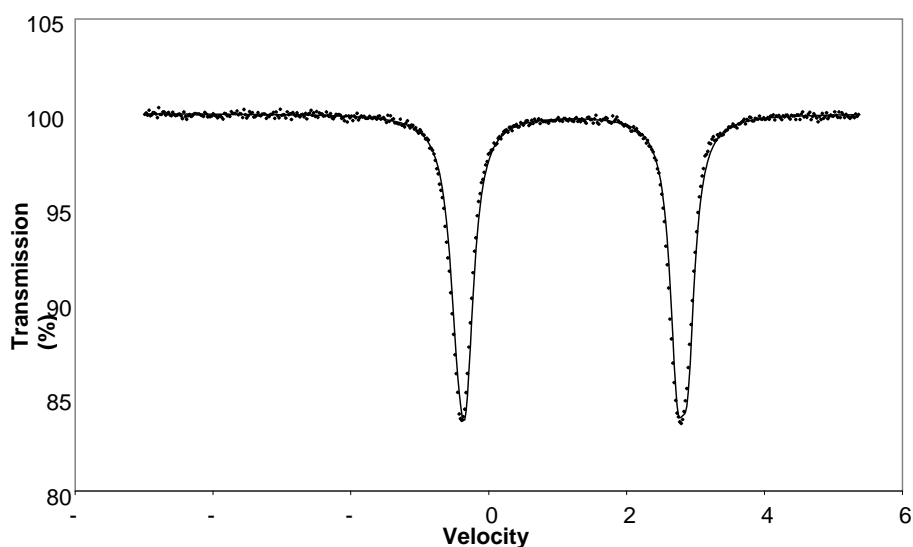
Figure S3. Mössbauer spectrum of **1** recorded at 80 K shown together with a fit obtained with a two doublets model.
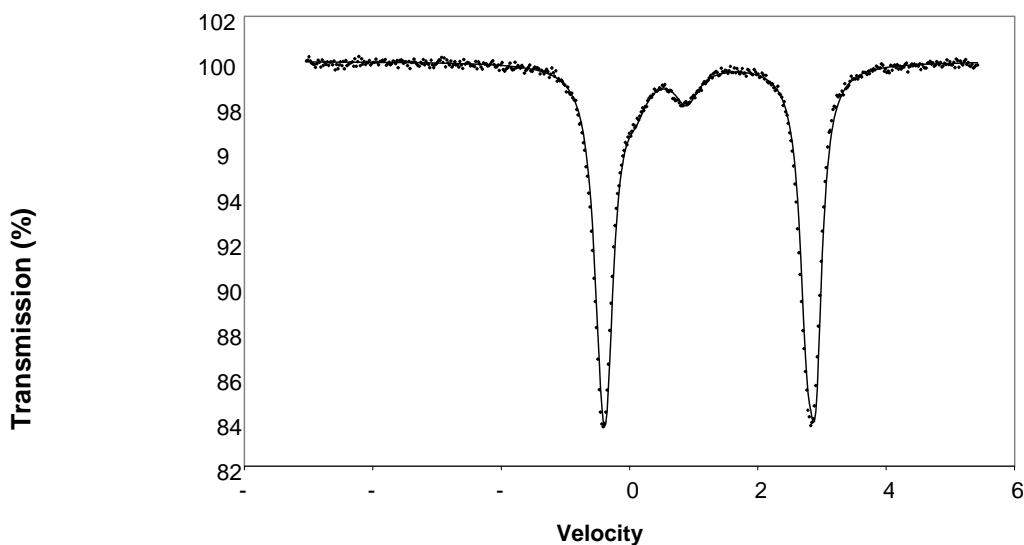
Figure S4 Mössbauer spectrum of **2** recorded at 80 K shown together with a fit obtained with a two doublets model.

Table S3. Mössbauer fits parameters for complex **1**.

Complex **1**	i.s.	q.s.	h.w.h.m.	Abundance
One doublet	1.19	3.18	0.17	100
Two doublet (overlapped)	1.24	3.18	0.14	66
	1.10	3.18	0.13	34
Two doublet (nested)	1.19	3.35	0.13	39
	1.19	3.07	0.14	61

Table S4. Mössbauer fits parameters for complex **2** and an impurity in the sample.

Complex **2** (with impurity)	i.s.	q.s.	h.w.h.m.	Abundance
One doublet	1.20	3.23	0.17	90
(impurity)	0.52	0.74	0.22	10
Two doublet (overlapped)	1.24	3.24	0.14	62
	1.11	3.23	0.13	27
(impurity)	0.49	0.76	0.21	11
Two doublet (nested)	1.20	3.35	0.13	42
	1.20	3.12	0.14	47
(impurity)	0.50	0.75	0.21	11

i.s. = isomer shift; q.s. = quadrupole splitting; h.w.h.m = half-width at half-maxima.
Units = mm s^{-1}. Errors $\leq \pm 0.01$ mm s^{-1}.

3. Susceptibility and Magnetisation Measurements

Figure S5 shows magnetization measurements on restrained powders of **1** and **2**. The high-field (5 T) value is much less than that expected for and $S = 8$ system, which is due to zero-field splitting, see below.
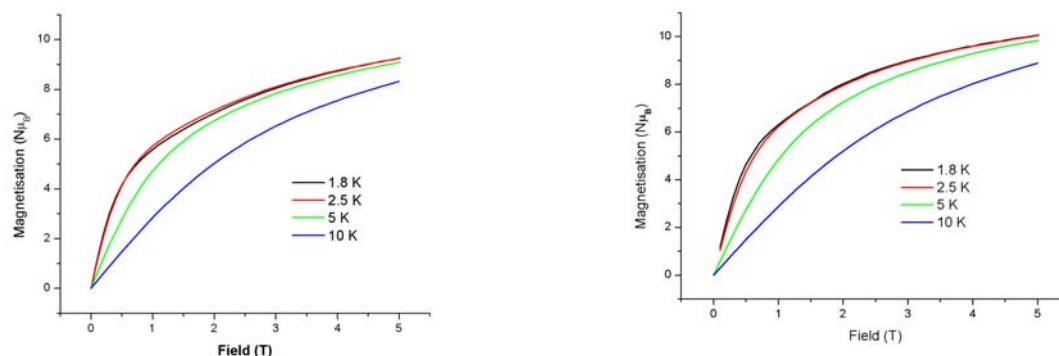
Figure S5. Magnetisation of complex **1** (left) and **2** (right) as a function of the magnetic field at different temperatures.

The susceptibility curves for **1** and **2** (Figure 2 in the main text) are very similar, showing ferromagnetic interactions, evidenced by the increase in χT upon lowering the temperature from room temperature, but a low temperature value ($\chi T = 16 - 17$ cm^{3}Kmol^{-1}) much below that expected for an $S = 8$ ground state ($\chi T = 32$ cm^{3}Kmol^{-1} for $g = 2$), even when taking into account zero-field splitting of the ground state. This appears to indicate the presence of antiferromagnetic interactions, or a ground state spin with $S < 8$. We assume (without conclusive proof) that the exchange interactions in the two complexes are similar in nature and strength. Compound **1** crystallises in an S_4 symmetry space group, and indeed the crystallographic cluster point group symmetry is S_4. However, there are two independent molecules in the unit cell. Bond angles, which are expected to determine nature and strength of the exchange interactions, are depicted in Figure S6. Indeed, the Fe$_1$–O–Fe$_2$ bond angle (and hence the Fe$_3$–O–Fe$_4$ bond angle) are more obtuse than the other Fe–O–Fe angles, suggesting that the J_1 interactions may be antiferromagnetic, while the J_2 interactions are antiferromagnetic. Theoretically, a second possibility is that all exchange interactions in one molecule are ferromagnetic, while all exchange interactions in the other molecule are antiferromagnetic, leading to $S = 8$ and $S = 0$ ground states respectively, while the average susceptibility could perhaps explain the low temperature χT value. No other ground states are possible in S_4 symmetry (Figure S7). The Heisenberg-exchange spin Hamiltonian for an S_4-symmetric cubane cluster reads (in the +J formulation):[3]

$$\mathcal{H}^{S_4} = J_1(\hat{\mathbf{S}}_1 \cdot \hat{\mathbf{S}}_2 + \hat{\mathbf{S}}_3 \cdot \hat{\mathbf{S}}_4) + J_2(\hat{\mathbf{S}}_1 \cdot \hat{\mathbf{S}}_3 + \hat{\mathbf{S}}_1 \cdot \hat{\mathbf{S}}_4 + \hat{\mathbf{S}}_2 \cdot \hat{\mathbf{S}}_3 + \hat{\mathbf{S}}_2 \cdot \hat{\mathbf{S}}_4)$$

with $J_1 = J_{12} = J_{34}$, and $J_2 = J_{13} = J_{14} = J_{23} = J_{24}$. The energies are then given by:

$$E^{S_4} = \tfrac{1}{2}J_1\left[S_{12}(S_{12}+1) + S_{34}(S_{34}+1) - 4S(S+1)\right] + \tfrac{1}{2}J_2\left[S_T(S_T+1) - S_{12}(S_{12}+1) - S_{34}(S_{34}+1)\right],$$

where S is the single ion spin ($S = 2$), and S_T the total spin of a state. Figure S7 shows the energies of the spin states as a function of the ratio J_1/J_2 for ferromagnetic J_2, with a crossover between $S = 0$ and $S = 8$ ground states at $J_1/J_2 = -0.8$. For antiferromagnetic J_2, the ground state is always $S = 0$.

In compound **2**, there is only one independent molecule in the unit cell, without particular symmetry. Assuming C_{2v} symmetry, again the energies of the spin states can be derived. The relevant spin Hamiltonian and energies are given by:[3]

$$\mathcal{H}^{C_{2v}} = J_{12}\hat{\mathbf{S}}_1 \cdot \hat{\mathbf{S}}_2 + J_{34}\hat{\mathbf{S}}_3 \cdot \hat{\mathbf{S}}_4 + J''(\hat{\mathbf{S}}_1 \cdot \hat{\mathbf{S}}_3 + \hat{\mathbf{S}}_1 \cdot \hat{\mathbf{S}}_4 + \hat{\mathbf{S}}_2 \cdot \hat{\mathbf{S}}_3 + \hat{\mathbf{S}}_2 \cdot \hat{\mathbf{S}}_4)$$

$$E^{S_4} = \tfrac{1}{2}J_{12}\left[S_{12}(S_{12}+1) - 2S(S+1)\right] + \tfrac{1}{2}J_{34}\left[S_{34}(S_{34}+1) - 2S(S+1)\right] +$$
$$\tfrac{1}{2}J''\left[S_T(S_T+1) - S_{12}(S_{12}+1) - S_{34}(S_{34}+1)\right]$$

with $J' = J_{13} = J_{14} = J_{23} = J_{24}$. Figure S7 shows the ground state obtained as a function of J_{12} and J_{34} for ferromagnetic J', demonstrating the possibility to obtain a spin ground state with intermediate spin in this case.

However, assuming the exchange interactions to be similar in both molecules, i.e. the same model to apply for both complexes, the presence of only one independent molecule in **2** excludes the possibility of different ground states for the two molecules in **1**, while the high point group symmetry of **1** excludes an intermediate ground state in **1**. Hence, the only possible model that is applicable to both **1** and **2** is therefore that of competing ferro- and antiferromagnetic interactions.
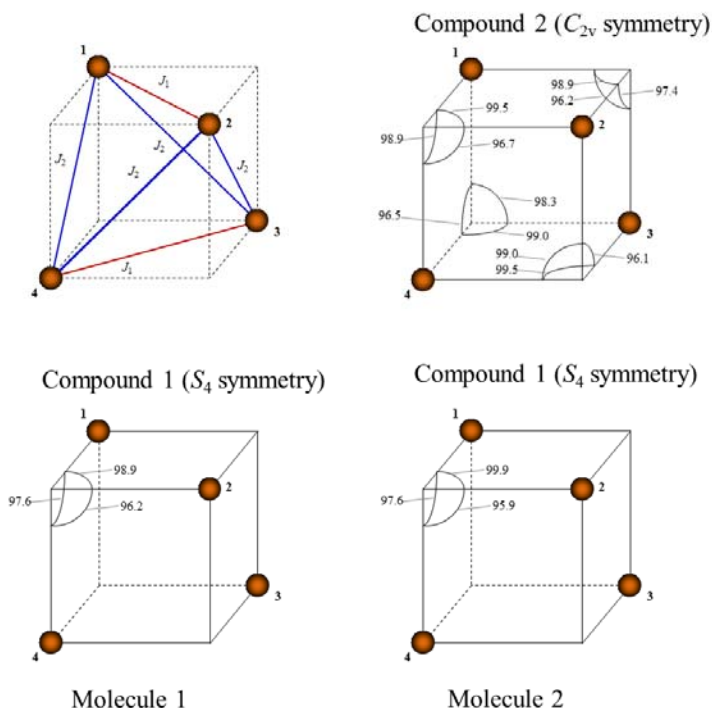
Figure S6. The used model to fit the susceptibility and magnetisation data, as well as the actual Fe–O–Fe bond angles in **1** and **2**.
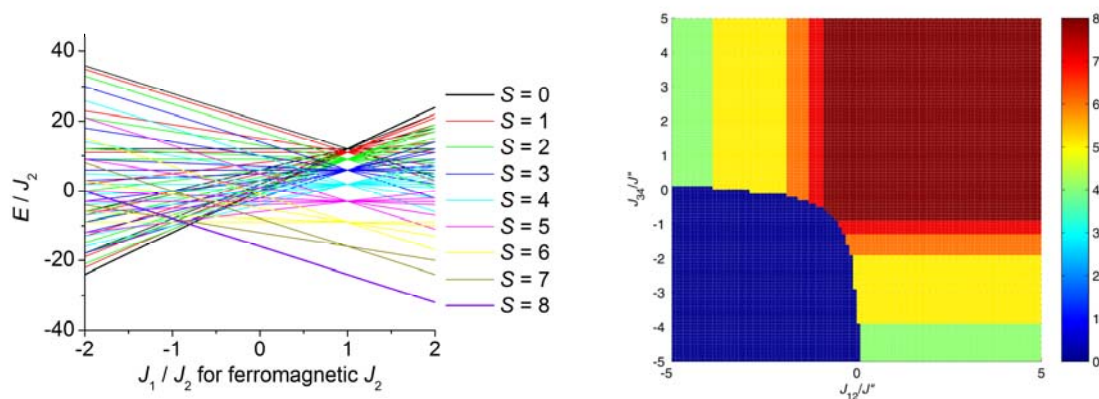
Figure S7 Left: Spin state energy as a function of J_1/J_2 for ferromagnetic J_2 (S_4 symmetry); Right: Ground state spin as a function of of J_{12}/J' and J_{34}/J' for ferromagnetic J' (C_{2v} symmetry), where $J'=J_{13}=J_{14}=J_{23}=J_{34}$.

Extensive simulations of both the susceptibility and the magnetisation for both **1** and **2** were carried out by employing the MAGPACK programme, assuming one independent molecule and S_4 symmetry, both to avoid overparametrisation. The MAGPACK programme uses the $-2J$ convention for the isotropic exchange spin Hamiltonian.[4] The model includes single-ion zero-field splitting (ZFS), with the assumption that the single-ion ZFS quantisation axes are all collinear with the molecular quantisation axis. Given that there is no particular reason for this assumption to be valid, the obtained single-ion D values should be taken as order-of-magnitude estimates. The spin Hamiltonian is then:

$$\mathcal{H} = -2J_1(\hat{\mathbf{S}}_1 \cdot \hat{\mathbf{S}}_2 + \hat{\mathbf{S}}_3 \cdot \hat{\mathbf{S}}_4) - 2J_2(\hat{\mathbf{S}}_1 \cdot \hat{\mathbf{S}}_3 + \hat{\mathbf{S}}_1 \cdot \hat{\mathbf{S}}_4 + \hat{\mathbf{S}}_2 \cdot \hat{\mathbf{S}}_3 + \hat{\mathbf{S}}_2 \cdot \hat{\mathbf{S}}_4) + D\sum_{i=1}^{4} \hat{S}_{z,i}$$

Figure S8 shows the dependence of the simulated magnetic susceptibility on the single ion D value, as well as the experimental data for **1**, as an example. Considering the approximations in the model, a good-quality fit is obtained for $J_1 = -1.4$ cm^{-1}, $J_2 = +1.7$ cm^{-1}, $D = 8$ cm^{-1} and $g = 2$. The susceptibility and magnetisation curves for **2** look very similar, where repeated measurements show the discrepancy to be within the experimental error, given that the sample is weighed out in the glove box. The obtained energy level diagram (Figure S9) does not show a clear ground state with a well-defined ZFS, in which case a quadratic M_S-energy dependence of the $\pm M_S$ states would be expected.
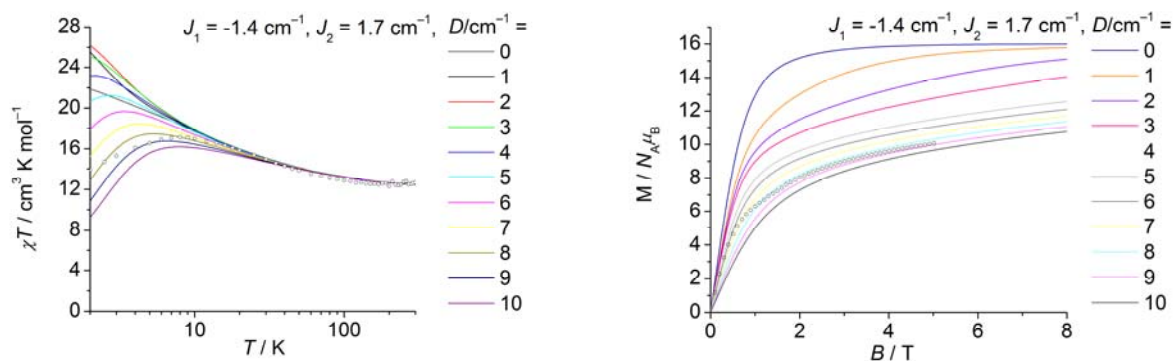
Figure S8 Magnetic susceptibility (left) and magnetisation (right) simulations as well as the experimental data for **1**.
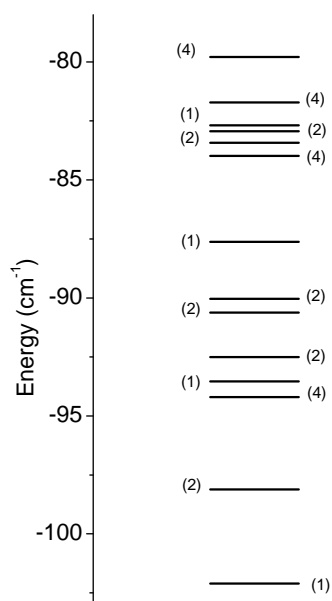
Figure S 9 Energy level diagram obtained for $J_1 = -1.4$ cm^{-1}, $J_2 = +1.7$ cm^{-1}, $D = 8$ cm^{-1} and $g = 2$, where the multiplicities of the levels are given in parentheses.

4. MCD measurements

Figure S11 displays the MCD spectra of a dichloromethane/ethanol (1:1) solution of complex 2 at 5 K and 6 T, before and after exposure to air. These spectra show that the bands at 18000 and 19500 cm^{-1} are due to Fe(III) impurities deriving from partial decomposition/oxidation of the sample.
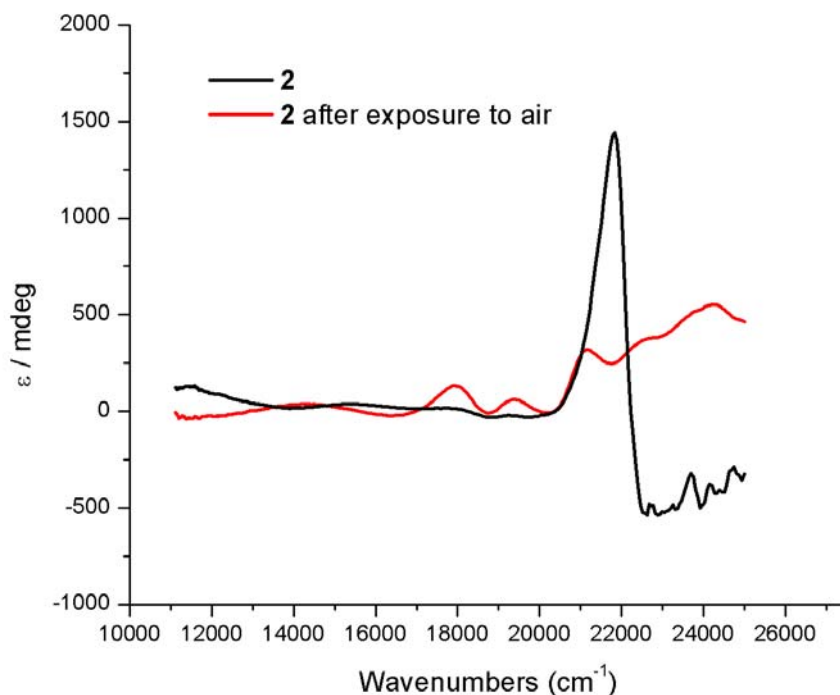
Figure S 10 MCD spectra recorded on a dichloromethane/ethanol (1:1) solution of complex **2** at 5 K and 6 T, before and after exposure to air.

References

1. G. M. Sheldrick, *Acta Cryst., Sect. A*, 2008, **64**, 112.
2. J. F. Duncan, R. M. Golding, *Quarterly Reviews*, 1965, **19**, 36.
3. A. Bencini, D. Gatteschi, *EPR of exchange coupled systems*, Springer-Verlag, Berlin, 1990.
4. J. J. Borras-Almenar, J. M. Clemente-Juan, E. Coronado, B. S. Tsukerblat, *J. Comp. Chem.*, 2001, **22**, 985.